Supplement of Atmos. Chem. Phys., 19, 8669–8686, 2019
https://doi.org/10.5194/acp-19-8669-2019-supplement
© Author(s) 2019. This work is distributed under
the Creative Commons Attribution 4.0 License.

Atmospheric Chemistry and Physics
Open Access
EGU

Supplement of

Impact of El Niño–Southern Oscillation on the interannual variability of methane and tropospheric ozone

Matthew J. Rowlinson et al.

Correspondence to: Matthew J. Rowlinson (ee11mr@leeds.ac.uk)

The copyright of individual parts of the supplement might differ from the CC BY 4.0 License.

Supplementary material

Methane Box Model

The effect of changes to global OH concentrations on global mean surface CH_4 concentrations is calculated in a simple global box model using the following equation:

$$\frac{1}{\Delta t}(X_{t+\Delta t} - X_t) = E - L = E - k[OH][X] \qquad (1)$$

where, X = global mean CH_4 in ppb, E = Annual emissions in Tg yr^{-1}, L = chemical loss to reaction with OH in Tg yr^{-1} and k = rate constant for reaction CH_4 + OH (k = 2.45×10^{-12} cm^3 $molecule^{-1}$ yr^{-1}) (Sander et al., 2011).

The model uses equation 1 to integrate global mean CH_4 based on annual mean emissions and chemical loss in time steps of 1 month. The relevant CH_4 emissions and monthly mean tropospheric OH concentrations from each simulations were applied to the box model. McNorton et al. (2016) found that using annually varying temperature had a very small effect on derived concentrations, therefore a constant temperature of 272.9 K was used.

Figure S1.

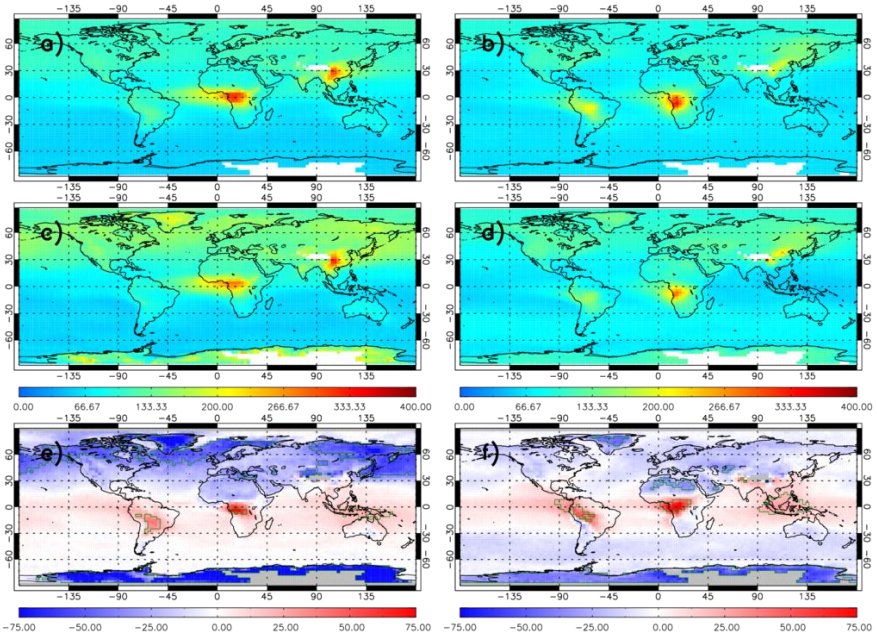

Figure S1: Carbon Monoxide (CO) at 800 hPa seasonal averages for 2007-2008 in ppb. a) TOMCAT (December-January-February, DJF), b) TOMCAT (June-July-August, JJA), c) MOPITT DJF, d) MOPITT JJA, e) TOMCAT – MOPITT mean bias DJF and f) TOMCAT – MOPITT mean bias JJA. Green polygons in panels e-f show regions where the absolute model-satellite mean bias is greater than the satellite uncertainty (Emmons et al., 2004; Monks et al., 2017).

Figure S2.

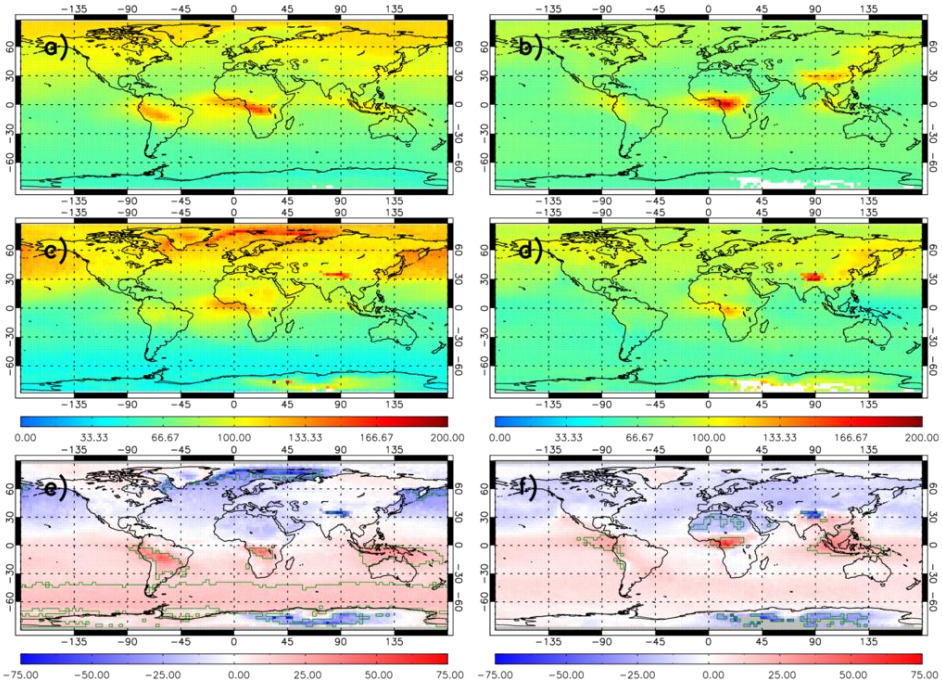

Figure S2: Carbon Monoxide (CO) at 500 hPa seasonal averages for 2007-2008 in ppb. a) TOMCAT (December-January-February, DJF), b) TOMCAT (June-July-August, JJA), c) MOPITT DJF, d) MOPITT JJA, e) TOMCAT – MOPITT mean bias DJF and f) TOMCAT – MOPITT mean bias JJA. Green polygons in panels e-f show regions where the absolute model-satellite mean bias is greater than the satellite uncertainty (Emmons et al., 2004; Monks et al., 2017).

Carbon Monoxide Retrievals:

The Measurement of Pollution in the Troposphere (MOPITT) instrument is on-board NASA's EOS Terra satellite, launched in March 2000 (Emmons et al., 2004). MOPITT is nadir viewing with an over pass time of approximately 10.00 local time (LT) and a swath footprint of 22 km x 22 km. It has eight channels measuring radiances: four in the thermal infrared (IR) near 4.7 μm and four in near IR using reflected solar radiation near 2.3 μm (Emmons et al., 2004).

For direct comparison between TOMCAT and MOPITT CO, the satellite averaging kernels (AKs) need to be the model fields. This accounts for the vertical sensitivity of the instrument when retrieving CO profiles. The AK is applied to the model as:

$$\boldsymbol{y} = \mathbf{10.0}^{\boldsymbol{A}(\log_{10} x - \log_{10} x_a) - \log_{10} x_a}$$

where $\boldsymbol{y}$ is the modified model profile, $\boldsymbol{A}$ is the AK, $\boldsymbol{x}$ is the model profile interpolated onto the satellite vertical pressure grid and $\boldsymbol{x_a}$ is the apriori. Here, only satellite CO retrievals are used where the degrees of freedom (DOF) are > 1.0 (Monks et al., 2017).

Figure S3.

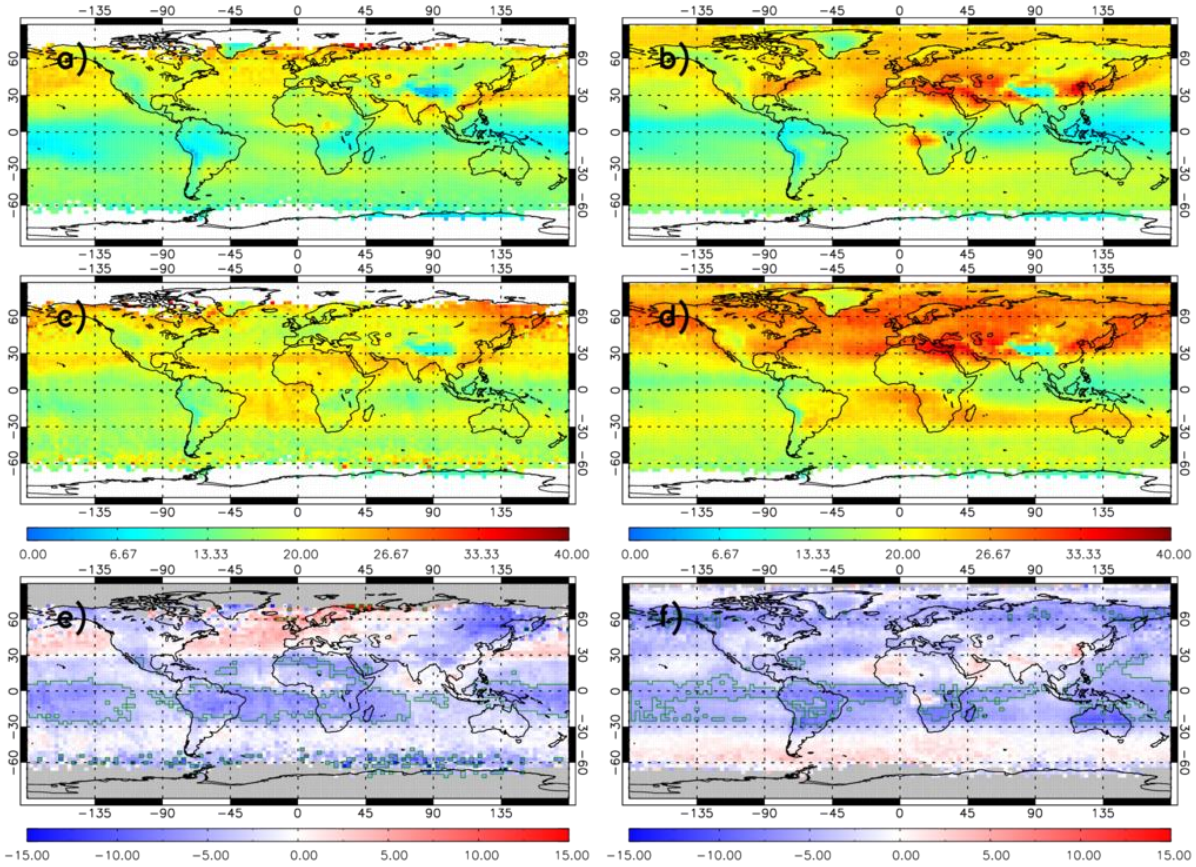

Figure S3: Sub-column (0-6 km) Ozone (O3) seasonal averages for 2007-2008 in Dobson units (DU). a) TOMCAT (December-January-February, DJF), b) TOMCAT (June-July-August, JJA), c) OMI DJF, d) OMI JJA, e) TOMCAT – OMI mean bias DJF and f) TOMCAT – OMI mean bias JJA. Green polygons in panels e-f show regions where the absolute model-satellite mean bias is greater than the satellite uncertainty (Miles et al., 2015).

Ozone retrievals:

The Ozone Monitoring Instrument (OMI) is on-board NASA's EOS-Aura satellite and has an overpass time of approximately 13.30 LT. It has a nadir viewing spectrum of 270-500 nm and has a central swath pixel size of 16-23 km (Boersma et al., 2011). The data has been screened for geometric cloud fraction of under 0.2, good data flags, the OMI row anomaly and where the solar zenith angle is greater than 80◦. The sub-column ozone (O_3) is based on an optimal estimation algorithm utilised by Miles et al. (2015).

The OMI sub-column O_3 AK is applied as:

$$\boldsymbol{y} = \boldsymbol{A}.\boldsymbol{x} + \boldsymbol{x_a}$$

where $\boldsymbol{A}$ is the AK and $\boldsymbol{x}$ is the model profile interpolated onto the satellite pressure grid and $\boldsymbol{x_a}$ is the apriori.

Figure S4.

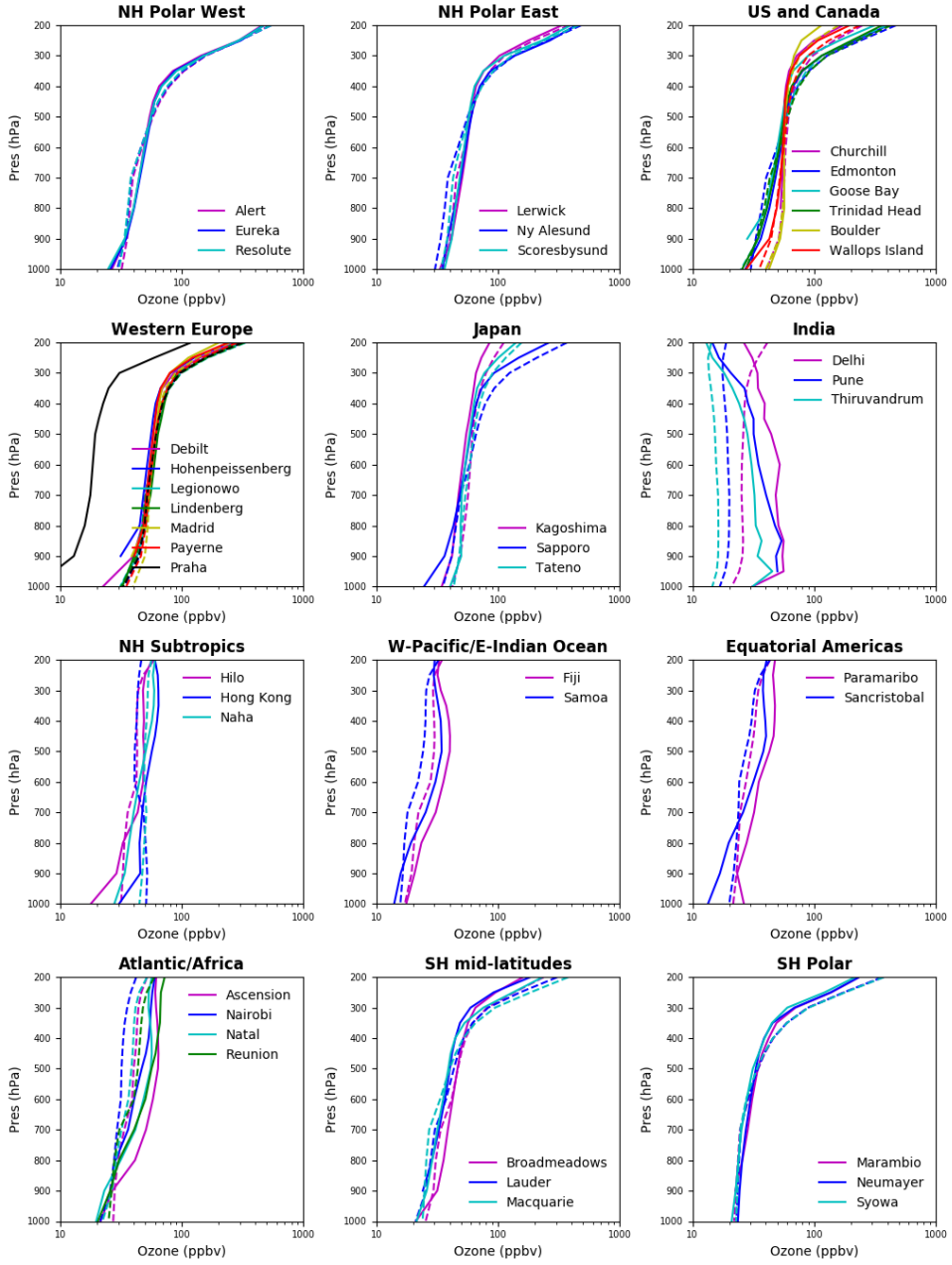

Figure S4: Comparison of annual mean ozone profiles from 1997-2011 simulated in TOMCAT (solid lines) against ozone sondes observations (dashed lines) from the Tilmes et al. (2012) climatology, 1995-2011.

Figure S5.

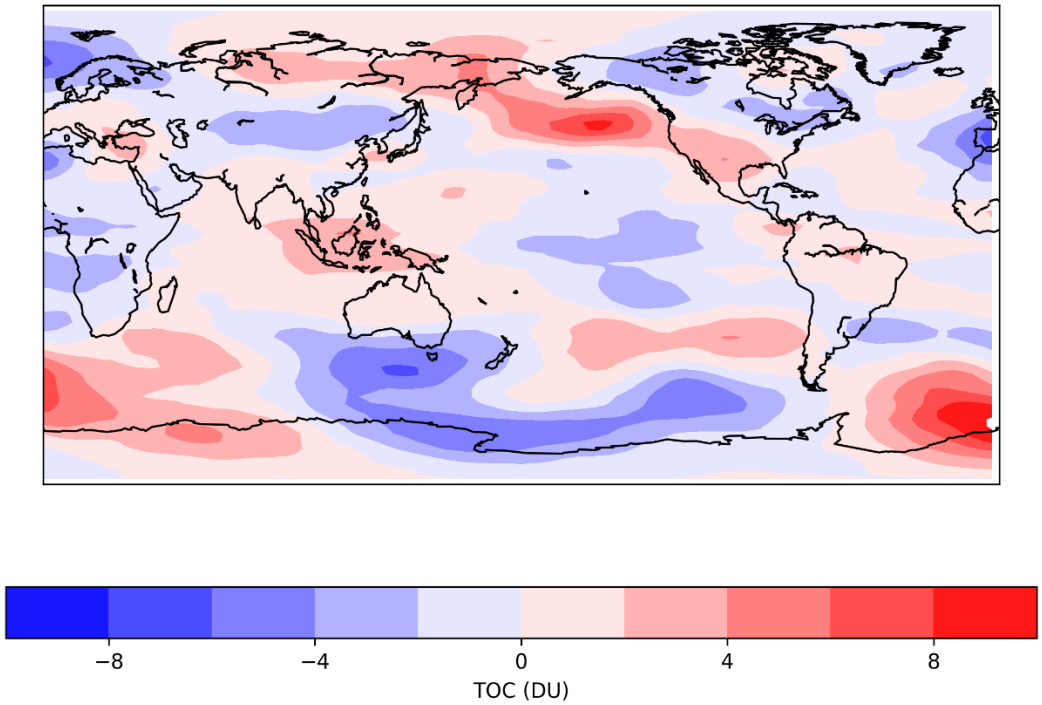

Figure S5: Difference in Total Ozone Column (TOC) during El Niño events compared to the 1995-2014 period mean.

Figure S6.

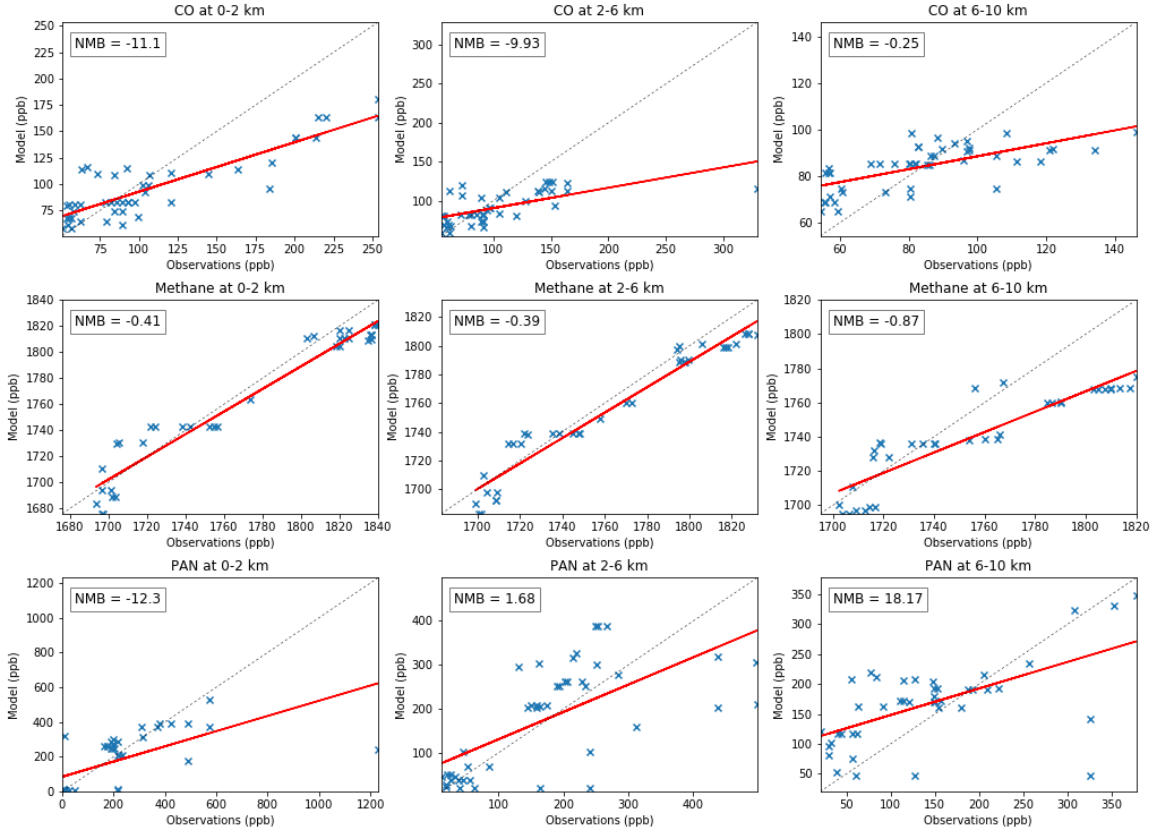

Figure S6. Comparison of annual global mean volume mixing ratios of CO (ppb), CH_4 (ppb) and PAN (ppt) from TOMCAT for the period 1993-2001 against aircraft observations that took place between 1992-2001, at 0-2 km (left panels), 2-6 km (middle panels) and 6-10 km (right panels). Normalised mean bias (NMB) values between the model and observations are shown in each panel.

Table S1 Aircraft campaign information from Emmons et al., (2010) climatologies.

Campaign	Date collected	Species	Location
TRACE-A	Sep 21 – Oct 26, 1992	O3, CO, NOx	East Brazil Coast (-35- -25N, 310-320E) East Brazil (-15- -5N, 310-320E) South Africa (-25- -5N, 15- 35E) South Atlantic (-20-0N, 340-350E) West Africa Coast (-25- -5N, 0-10E)
PEM-West-B	Feb 7 – Mar 14, 1994	CO, NOx	China Coast (20-30N, 115-130E) Japan (25-40N, 135-150E) Philippine Sea (5-20N, 135-150E)
TOTE	Dec 6 – 22, 1995	O3, CO, CH4	Alaska (60-70N, 205-220E) Hawaii (15-25N, 195-210N)
VOTE	Jan 20 – Feb 19, 1996	O3, CO, CH4	Alaska (60-70N, 205-220E) Hawaii (15-25N, 195-210N)
SUCCESS	Apr 15 – May 15, 1996	O3, CO	Central USA (35-40N, 260-265E)
PEM-Tropics-A	Aug 15-Oct 15, 1996	O3, CO, CH4, NOx	Christmas Island (0-10N, 200-220E) Easter Island (−40- −20N, 240-260E) Hawaii (10-30N, 190- 210E) Tahiti (−20- 0N, 200-230E)
POLINAT-2	Sep 19 – Oct 25, 1997	O3, CO, NOx	Canary Islands (25-35N, 340-350E) Eastern Atlantic (35-45N, 330-340E) Europe (45-55N, 5-15E) Ireland (50-60N, 345-355E)
SONEX	Oct 7 – Nov 12, 1997	O3, CO	East Atlantic (35-45N, 325-345E) Ireland (50-60N, 345-355E) Newfoundland (45-55N, 290-310E)
PEM-Tropics-B	Mar 6 – Apr 18, 1999	O3, CO, CH4, NOx	Christmas Island (0-10N, 200-220E) Easter Island (−40- −20N, 240-260E) Fiji (-30- -10N, 170-190E) Hawaii (10-30N, 190- 210E) Tahiti (−20- 0N, 200-230E
TOPSE	Feb 5 – May 23, 2000	O3, CH4, NOx	Boulder (37- 47N, 250-270E) Churchill (47-65N, 250-280E) Thule (65-90N, 250-300E)
TRACE-P	Feb 24 – Apr 10, 2001	O3, CO, CH4, NOx	China (10-30N, 110-130E) Guam (10-20N, 140-150E) Hawaii (10-30N, 190-210E) Japan (20-40N, 130-150E)

References

Boersma, K., Eskes, H., J. Dirksen, R., van der A, R., Veefkind, P., Stammes, P., Huijnen, V., L. Kleipool, Q., Sneep, M., Claas, J., Leitão, J., Richter, A., Zhou, Y., and Brunner, D.: An improved tropospheric NO2 column retrieval algorithm for the Ozone Monitoring Instrument, 2329-2388 pp., 2011.

Emmons, L. K., Deeter, M. N., Gille, J. C., Edwards, D. P., Attié, J.-L., Warner, J., Ziskin, D., Francis, G., Khattatov, B., Yudin, V., Lamarque, J.-F., Ho, S.-P., Mao, D., Chen, J. S., Drummond, J., Novelli, P., Sachse, G., Coffey, M. T., Hannigan, J. W., Gerbig, C., Kawakami, S., Kondo, Y., Takegawa, N., Schlager, H., Baehr, J., and Ziereis, H.: Validation of Measurements of Pollution in the Troposphere (MOPITT) CO retrievals with aircraft in situ profiles, Journal of Geophysical Research: Atmospheres, 109, doi:10.1029/2003JD004101, 2004.

McNorton, J., Chipperfield, M., Gloor, M., Wilson, C., Wuhu, F., Hayman, G., Rigby, M., B. Krummel, P., O'Doherty, S., Prinn, R., Weiss, R., Young, D., Dlugokencky, E., and Montzka, S. A.: Role of OH variability in the stalling of the global atmospheric CH4 growth rate from 1999 to 2006, 1-24 pp., 2016.

Miles, G. M., Siddans, R., Kerridge, B. J., Latter, B. G., and Richards, N. A. D.: Tropospheric ozone and ozone profiles retrieved from GOME-2 and their validation, Atmos. Meas. Tech., 8, 385-398, 10.5194/amt-8-385-2015, 2015.

Monks, S., R. Arnold, S., Hollaway, M., Pope, R., Wilson, C., Wuhu, F., Emmerson, K., J. Kerridge, B., Latter, B., M. Miles, G., Siddans, R., and P. Chipperfield, M.: The TOMCAT global chemical transport model v1.6: Description of chemical mechanism and model evaluation, 3025-3057 pp., 2017.

Sander, S. P., Abbatt, J., Barker, J., Burkholder, J. B., Friedl, R. R., Golden, D. M., Huie, R., Kurylo, M., Moortgat, G., Orkin, V., and Wine, P.: Chemical Kinetics and Photochemical Data for Use in Atmospheric Studies, Evaluation No. 17, 2011.

Tilmes, S., Lamarque, J. F., Emmons, L. K., Conley, A., Schultz, M. G., Saunois, M., Thouret, V., Thompson, A. M., Oltmans, S. J., Johnson, B., and Tarasick, D.: Ozonesonde climatology between 1995 and 2011: description, evaluation and applications, Atmos. Chem. Phys., 12, 7475-7497, 10.5194/acp-12-7475-2012, 2012.